FEBS Letters 588 (2014) 443–449

FEBS Letters

journal homepage: www.FEBSLetters.org

Sphingolipid levels crucially modulate lateral microdomain organization of plasma membrane in living yeast

Jaroslav Vecer [a], Petra Vesela [b], Jan Malinsky [b,*], Petr Herman [a,*]

[a] Faculty of Mathematics and Physics, Charles University, Ke Karlovu 5, 121 16 Prague 2, Czech Republic
[b] Institute of Experimental Medicine, Academy of Sciences of the Czech Republic, Videnska 1083, 142 20 Prague 4, Czech Republic

ARTICLE INFO

Article history:
Received 15 November 2013
Accepted 29 November 2013
Available online 12 December 2013

Edited by Sandro Sonnino

Keywords:
Membrane microdomain
Lipid order
Fluidity
Fluorescence anisotropy
Time-resolved fluorescence

ABSTRACT

We report sphingolipid-related reorganization of gel-like microdomains in the plasma membrane of living *Saccharomyces cerevisiae* using *trans*-Parinaric acid (t-PnA) and 1,6-diphenyl-1,3,5-hexatriene (DPH). Compared to control, the gel-like domains were significantly reduced in the membrane of a sphingolipid-deficient *lcb*1-100 mutant. The same reduction resulted from sphingolipid depletion by myriocin. The phenotype could be reverted when a myriocin-induced block in sphingolipid biosynthesis was bypassed by exogenous dihydrosphingosine. Lipid order of less-ordered membrane regions decreased with sphingolipid depletion as well, as documented by DPH fluorescence anisotropy. The data indicate that organization of lateral microdomains is an essential physiological role of these structural lipids.

1. Introduction

Sphingolipids (SL) are structural lipids involved in many physiologically important cell signaling cascades [1,2]. In ternary mixtures with phospholipids and sterols, SL form bilayers which can adopt, depending on abundance of individual components, several structural arrangements corresponding to different thermodynamic phases: in gel (solid ordered, S_o) phase, lipid molecules containing long acyl chains in *all-trans* conformation (mainly sphingolipids) are tightly arranged in a 2D crystalline lattice, while lipids in liquid phases undergo free lateral diffusion. According to the average conformation of phosphoglycerol- and SL acyl chains, liquid disordered (L_d) and sterol-enriched liquid ordered (L_o) phase are further distinguished [3].

It seems evident nowadays that biological membranes exhibit microdomain organization, too. Local protein and lipid accumulations are supposed to generate differential microenvironments, in which specific biological functions are executed [4,5]. Various mechanisms of lateral domain formation have been formulated to date [6,7]. The most popular, so called 'lipid raft' theory anticipates that lateral microdomains exhibiting order characteristics of L_o and L_d phases coexist under physiological conditions, L_o (raft) fraction being based on unspecific sterol-SL binding ([5] and references therein). Increasing evidence is being accumulated, however, that bipartite segmenting to raft and non-raft fraction is not enough to describe in full the appearance of biological membranes. Instead, more complex views of the membrane admitting numerous types of microdomains are arising [8,9]. In particular, presence of S_o phase, gel-like microdomains in the plasma membrane has been indicated [10–12]. Their possible enrichment in monohydroxylated ceramides [13], but not sterols has been reported [14].

Employing fluorescence intensity and anisotropy decays of 1,6-diphenyl-1,3,5-hexatriene (DPH) and *trans*-parinaric acid (t-PnA), we monitor changes in membrane order and the abundance of highly ordered S_o domains. To our best knowledge, we report the first measurements of the t-PnA time-resolved fluorescence anisotropy in living cells. Using SL-depleted cells and the same cells with SL levels replenished by exogenous sphingoid bases, we bring unequivocal evidence that S_o microdomains in the plasma membrane of living *Saccharomyces cerevisiae* are composed of sphingolipids. Participation of these structural lipids in regulation of membrane order outside S_o microdomains is strongly indicated.

2. Materials and methods

2.1. Cell strains and growth conditions

We used *S. cerevisiae* strains RH1800 (denoted as wild type; MATα *leu*2 *trp*1 *ura*3 *lys*2 *bar*1) and RH3804 (*lcb*1-100; MATα

Abbreviations: t-PnA, *all-trans*-9,11,13,15-octadecatetraenoic acid; DPH, 1,6-diphenyl-1,3,5-hexatriene; DHS, DL-dihydrosphingosine

* Corresponding authors. Fax: +420 241062597 (J. Malinsky), +420 224922797 (P. Herman).
E-mail addresses: malinsky@biomed.cas.cz (J. Malinsky), herman@karlov.mff.cuni.cz (P. Herman).

0014-5793/$36.00
http://dx.doi.org/10.1016/j.febslet.2013.11.038

*lcb*1-100 *leu*2 *trp*1 *ura*3 *lys*2 *bar*1) from H. Riezman. Cells were grown in a synthetic minimal medium (0.67% Difco yeast nitrogen base without amino acids, 2% glucose and essential amino acids) to an early log phase (optical density $OD_{600nm} = 0.5$). In all experiments including *lcb*1-100 strain, the cultivation was performed at 25 °C. Otherwise, cells were cultivated at 30 °C.

2.2. Cell staining

Cells were gently collected, washed (3×) in sterile water and resuspended in 10 mM MES (2-[*N*-morpholino]ethanesulphonic acid) buffer, pH = 6.0, to $OD_{600nm} = 0.5$. The cell suspension in a cuvette was stained by an addition of a stock solution of DPH in methanol to the final DPH concentration of 1.5 μM. The suspension was then incubated for 20 min at 25 °C. Alternatively, a small aliquot of stock solution of t-PnA in ethanol was added to the final concentration of 150 nM and cells were incubated for 6 min. In all cases, the fluorescence measurement immediately followed the staining procedure. Measurements of the unstained cell suspension right before the addition of the dye was always performed under exactly the same conditions. This procedure avoided any cell-concentration mismatch and allowed for an accurate correction of background fluorescence. Samples were continuously stirred during both the staining and data collection. Fresh suspension was used for each measurement and exposure of samples to light was minimized.

2.3. Time-resolved fluorescence

Fluorescence intensity and anisotropy decays were measured on an apparatus comprised of a laser excitation and a time-correlated single photon counting detection (Becker & Hickel, SPC150) with a cooled MCP-PMT (Hamamatsu, R3809U-50). t-PnA emission was excited at 318 nm by the third harmonic of the Ti:Sapphire laser (Coherent, Chameleon Ultra II). t-PnA emission was collected at 420 nm using a H-20 monochromator (HORIBA, Jobin-Yvon) equipped with a stack of 435/40 bandpass filter (Semrock, IL) and a long-pass filter (405 nm) placed in front of the input slit. DPH was excited at 355 nm, emission was isolated at 430 nm using the same monochromator and filter combination. All experiments were performed at 23 °C.

Intensity decays were acquired under magic-angle conditions, polarized components required for construction of the fluorescence anisotropy were accumulated quasi-simultaneously with a switching frequency of 30 s.

2.4. Associated anisotropy decays

Anisotropy decays of t-PnA were fitted by the associative model describing fluorescence depolarization in heterogeneous systems [15]. t-PnA partitioning between the liquid (L) and gel (G) phases was supposed to exhibit monoexponential anisotropy decay $r_L(t)$ and $r_G(t)$, respectively, with distinct correlation times and limiting anisotropies:

$$r_L(t) = r_0 \cdot \exp(-t/\phi_L) + r_{\infty,L} \quad \text{and} \quad r_G(t) = r_0 \cdot \exp(-t/\phi_G) + r_{\infty,G} \tag{1}$$

Overall anisotropy decay from a mixture of both environments is given by the additivity law:

$$r(t) = f_G \cdot r_G(t) + f_L \cdot r_L(t) \tag{2}$$

where $f_L(t)$ and $f_G(t)$ are time-dependent intensity fractions of t-PnA in the respective phases. The fractions were evaluated from measured fluorescence decays using Supplementary Eq. (S4) and kept fixed. The adjustable parameters were correlation times (ϕ_G and ϕ_L), limiting anisotropies ($r_{\infty,G}$ and $r_{\infty,L}$) and r_0 only.

3. Results

3.1. Plasma membrane of sphingolipid-depleted cells is less ordered compared to wild type

Sphingolipids were shown to significantly affect physical membrane properties and domain organization in liposomes [16,17]. Since the amount of SL in plasma membrane is carefully controlled [1], we asked whether it affects lateral membrane organization in living cells as well. We therefore probed plasma membranes of control and SL-depleted cells by 1,6-diphenylhexatriene (DPH), a lipophilic dye widely used in membrane order studies [18]. We analyzed emission and fluorescence anisotropy decays of DPH-stained suspension of the thermosensitive deletion strain *lcb*1-100 [19] and compared them to those of wild type. Essential *LCB*1 gene encodes a subunit of serine palmitoyltransferase, a key enzyme complex in the SL biosynthesis pathway (Fig. 1), and is required for its activity. In *lcb*1-100 cells the SL biosynthesis is blocked under heat-stress conditions (37 °C) and even at the permissive temperature of 24 °C the amount of SL drops to 38% of the wild type value [20].

Time-resolved fluorescence anisotropies of DPH in *lcb*1-100 and wild type cells are presented in Fig. 2. Rotational constraint of DPH is reflected in the limiting anisotropy r_∞, lower r_∞ indicates higher rotational freedom and lower lipid-chain order [21]. We detected significantly decreased r_∞ in the *lcb*1-100 cells compared to the wild type being 0.086 ± 0.003 and 0.106 ± 0.003, respectively (Fig. 2). Correlation times ϕ reflecting rotational diffusion of the probe (Supplementary Table S1) as well as DPH emission decays (Supplementary Table S2) remained essentially unchanged after the SL depletion. Our data show that although the chemical microenvironment of DPH is similar in plasma membranes of the two strains, *lcb*1-100 cells are unable to compensate for the loss of SL and exhibit reduced overall membrane order.

3.2. The amount of gel-like microdomains is reduced in the plasma membrane of lcb1-100 cells

Sphingolipids promote formation of highly ordered membrane domains in liposomes and artificial membranes [16,17,22,23]. Recently, it has been also suggested that they could be involved in

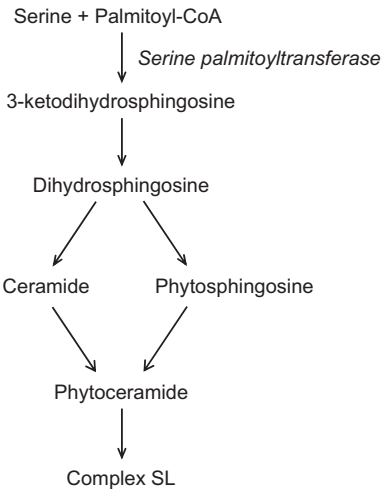

Fig. 1. Simplified biosynthetic pathway of yeast sphingolipids.

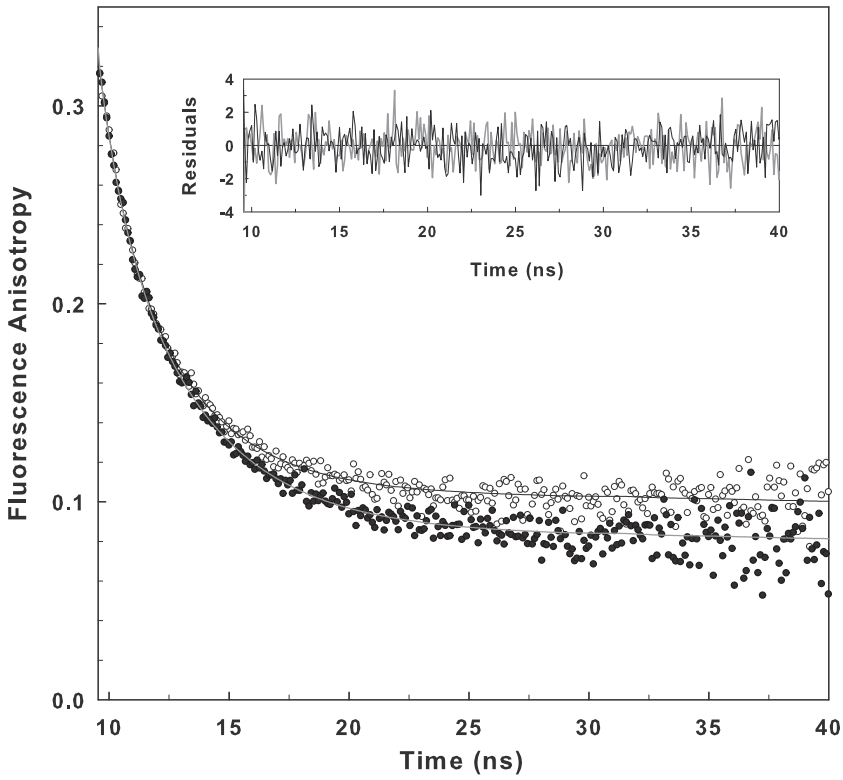

Fig. 2. Fluorescence anisotropy decays of DPH in plasma membranes of wild type (○) and *lcb*1-100 (●) cells. Solid lines represent the best fit.

formation of gel-like microdomains in plasma membranes of living cells [14]. We therefore compared relative abundance of the highly-ordered membrane environment in wild type and SL-depleted *lcb*1-100 cells using t-PnA.

t-PnA is a naturally occurring fluorescent fatty acid that has been extensively used for probing of lipid organization in simple lipid bilayers [17,24,25], and biomembranes [14,26]. Unlike other membrane probes, t-PnA possesses unique property of preferential partitioning into the highly-ordered gel phase with a partition coefficient of about five [17,24]. The probe is essentially non-fluorescent in water and exhibits characteristic quantum yields and lifetime components in fluid and gel phases. Fluorescence emission of t-PnA is complex, typically exhibiting several lifetime components even in homogenous solvents and pure lipid bilayers [25]. The decay complexity increases with heterogeneity of the membrane system, as demonstrated on liposomes with segregated fluid and gel phases [17,23]. Importantly, it has been unequivocally shown on variety of model membranes that partitioning of t-PnA to the gel phase is accompanied by an appearance of a new characteristic long-lived emission with lifetime longer than ~30–40 ns [16,22–24]. The longest lifetime component of t-PnA in membranes with Lo domains is somewhat shorter (25-30 nsec) that that in the gel state [17]. Due to its unique properties t-PnA represents an unparalleled tool for specific probing of the gel environment.

We found that emission decays of t-PnA in *lcb*1-100 and wild type cells significantly differ (Fig. 3). Decreased tail of the decay from *lcb*1-100 cells indicates significantly smaller fraction of long-lifetime components. In addition, parallel decay tails indicate similar lifetime values of these components. Detailed MEM analysis [27] of both *lcb*1-100 and wild type cells revealed four t-PnA emission decay components with lifetimes ranging from 2 to 55 ns (Table 1, Supplementary Fig. S1). While detailed assignment of shorter components is difficult, the longest and, in terms of intensity, the most abundant component with lifetime $\tau_G \sim 55$ ns can be safely assigned to t-PnA entrapped in a highly-ordered environment equivalent to gel-like domains [16,22–24]. Similar τ_G values above 50 ns were reported on liposomes where τ_G increased with a fraction of phosphoceramides [17,22]. As apparent from Table 1, decrease of the mean lifetime from 46 ns in wild type to 32 ns in *lcb*1-100 cells is caused mainly by dramatic reduction of the a_G amplitude. Since amplitudes are related to the amount of emitting species in the illuminated volume, this finding clearly indicates reduced amount of the ordered environment in *lcb*1-100 cells. The same τ_G values in both strains agree with this conclusion and indicate that the long-lived emission originates from similarly packed lipid environments.

To further support the observed reduction of the gel-like domains upon the SL depletion, we compared t-PnA fluorescence anisotropies of *lcb*1-100 and wild type cells. Both anisotropy decays depicted in Fig. 4 exhibit biphasic behavior that is a clear sign of membrane heterogeneity when probe with a phase-sensitive quantum yield partitions between phases with rather different fluidity and/or membrane order [15]. Similar t-PnA anisotropies were observed on mixed-lipid bilayers [15,25,28]. Importantly, both $r_{\infty,G}$ and $r_{\infty,L}$, and correlation times ϕ_G and ϕ_L belonging to the gel (G) and liquid (L) phases, respectively, can be extracted from the data [15,25]. As seen from the raw decays, r_∞ remains preserved in *lcb*1-100 and wild type cells. Since all short-lifetime components of the t-PnA decay are essentially extinct at times above 100 ns, the signal contributing to r_∞ belongs to τ_G and should originate from a highly ordered environment that displays the same lipid order in both strains. Fitting results from Table 2 confirm this finding and show that not only $r_{\infty,G}$ but also $r_{\infty,L}$ remains preserved upon SL depletion. The obtained r_∞ values of about 0.18 and 0.31, respectively, closely resemble those reported for fluid and solid phases on mixed-lipid bilayers [25,28]. This is significant independent evidence that the long lifetime component originates from the gel-like environment. Similar ϕ_G and ϕ_L values suggest comparable rotational diffusion rates of t-PnA in both environments and both cell types. It has to be noted that the proportion between the fluid

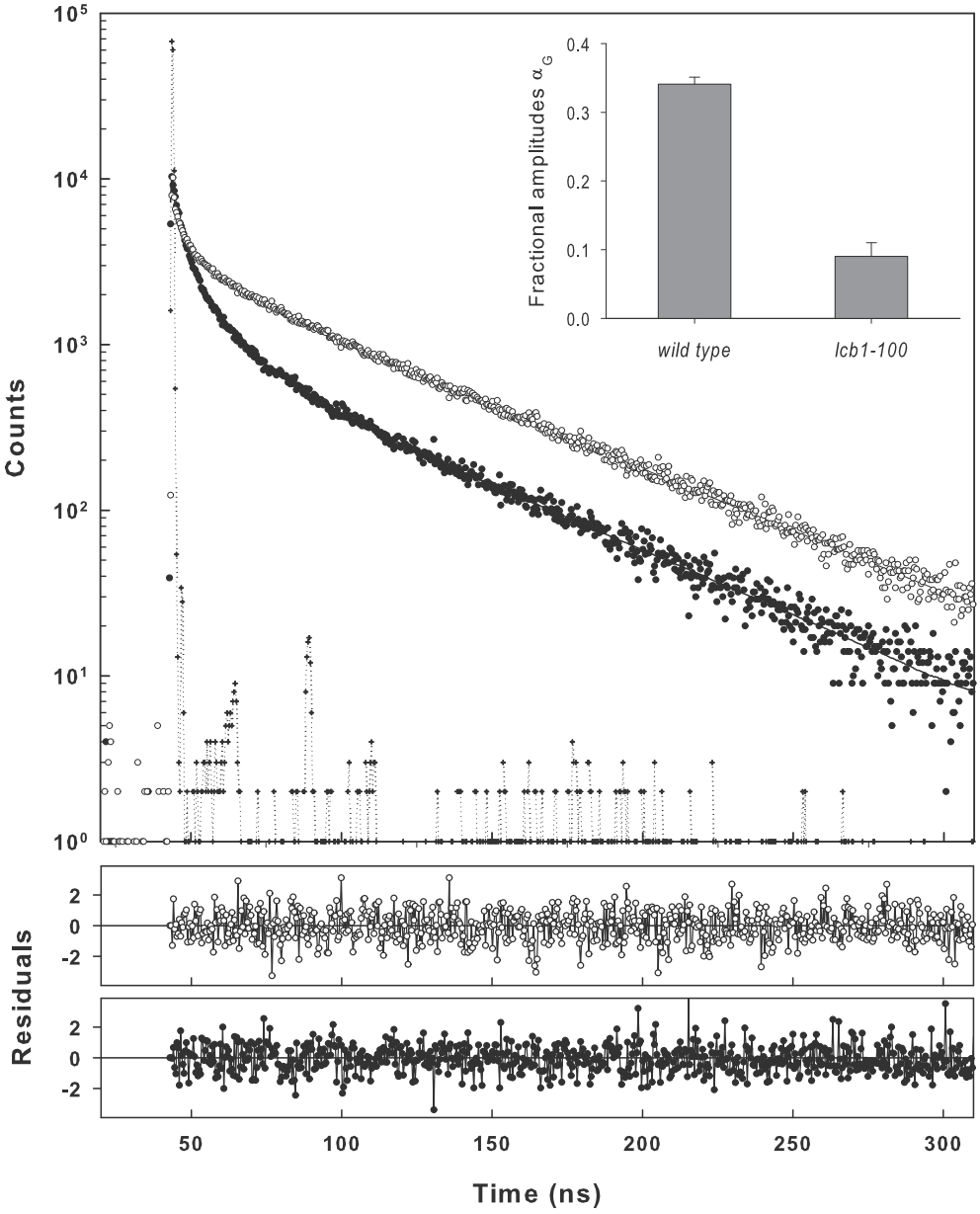

Fig. 3. Fluorescence decays of t-PnA in plasma membranes of wild type (○) and *lcb*1-100 cells (●). Solid lines represent the best fit and crosses impulse response function. Inset: fractional amplitudes of the gel-phase component.

Table 1
Fluorescence decay parameters of t-PnA in plasma membranes of wild type and *lcb*1-100 cells.

	τ_{mean} (ns)[a]	α_1	τ_1 (ns)	α_2	τ_2 (ns)	α_3	τ_3 (ns)	α_G	τ_G (ns)	f_G[d]
Wild type	46.2	0.27	2.2	0.30	7.4	0.09	21.1	**0.34**[b]	**54.6**	0.80
*lcb*1-100	31.7	0.45	2.5	0.31	5.7	0.15	15.0	**0.09**[c]	**54.8**	0.49

[a] τ_{mean} was calculated using Eq. (S3); S.D. < 0.05 ns.
[b] S.D. < 0.02.
[c] S.D. < 0.01.
[d] The intensity fraction was calculated using Supplementary Eq. (S4).

and the gel phases given by amplitudes α from Table 1 was fixed during the fitting. Since this represents a serious constraint, successful fit strongly indicates both an internal consistency of the model and correct assignment of t-PnA lifetimes to gel and fluid environment. Anisotropy data fully confirm conclusions from the lifetime analysis that the fraction, not properties of fluid and gel phases is altered in the plasma membrane of *lcb*1-100 cells.

3.3. Abundance of gel-like microdomains reflects specifically the variations in sphingolipid levels

Deletion of the *LCB*1 gene is lethal and even at the permissive temperature the *lcb*1-100 cells exhibit rather complex phenotype [19]. In order to exclude any possible interference resulting from the long-term metabolic adaptation of *lcb*1-100 cells, we

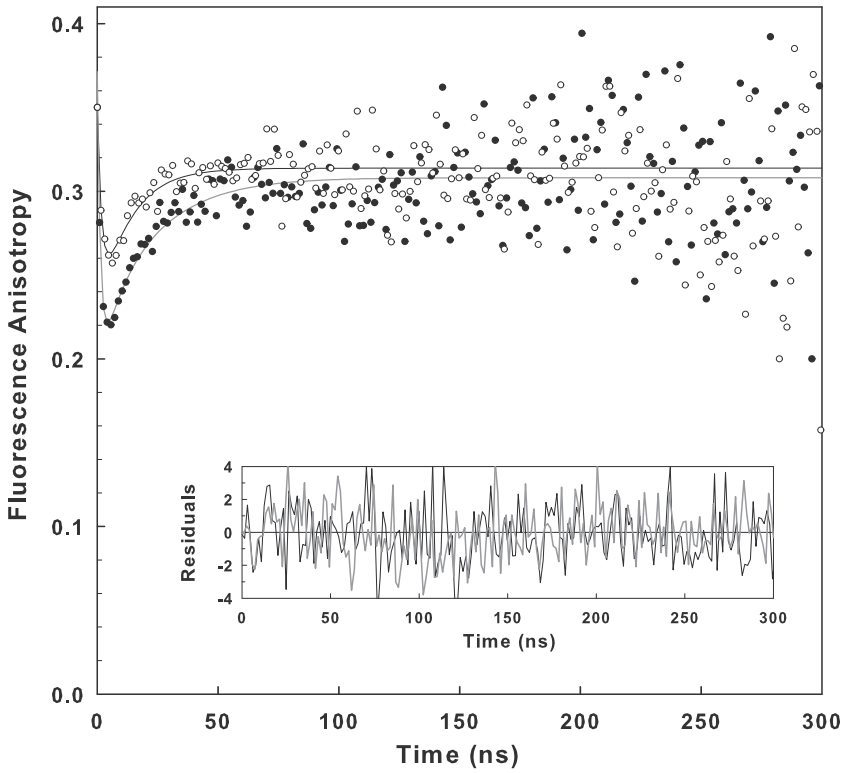

Fig. 4. Fluorescence anisotropy decays of t-PnA in plasma membranes of wild type (○, black line) and *lcb*1-100 cells (●, gray line). Solid lines represent the best fit.

Table 2
Fluorescence anisotropy decay parameters of t-PnA in plasma membranes of wild type and *lcb*1-100 cells.[a]

	r_0[b]	ϕ_G (ns)	ϕ_L (ns)	$r_{\infty,G}$[c,f]	$r_{\infty,L}$[c,f]
Wild type	0.35	2.2[d]	1.7[d]	0.314	0.176
*lcb*1-100	0.37	1.3[e]	1.1[e]	0.308	0.179

[a] Decay associated anisotropies were analyzed using t-PnA decay parameters from Table 1. α_G and τ_G were associated with the gel phase [16,17,25], the rest of the decay with the liquid phase.
[b] S.D. < 0.02.
[c] S.D. < 0.003.
[d] S.D. < 2 ns.
[e] S.D. < 5 ns.
[f] The second-rank order parameter <P_2> can be calculated as: $< P_2 >= \sqrt{r_\infty / r_0}$.

temporarily exposed wild type yeast to a sphingosine homolog myriocin, a specific inhibitor of serine palmitoyltransferase [29]. Since this enzyme catalyzes the first step of the sphingosine biosynthesis (Fig. 1), the myriocin treatment resulted in a rapid depletion of SL intermediates and a decrease in total membrane sphingolipids [30].

We found that myriocin treatment (2 h incubation with 5 μM myriocin) induced similar changes in fluorescence decay of t-PnA as deletion of the *LCB*1 gene (compare Fig. 5 and Fig. 3). While τ_G remained unchanged, 3-fold decrease in α_G after myriocin-induced SL depletion caused shortening of τ_{mean} from 49.1 to 40.5 ns (Table 3).

Block of SL biosynthesis by myriocin can be bypassed by addition of exogenous long-chain bases [29] . We therefore added to the myriocin-treated cells (2 h cultivation with myriocin) 20 μM DHS and incubated the culture for additional 2 h before measurements. The obtained results of this DHS supplement are shown in Fig. 5 and Table 3. Fig. 5 suggests that the long-decay component of t-PnA fluorescence becomes restored in DHS-supplied cells and its fraction even exceeds the wild type control. This observation is confirmed by values in Table 3. While τ_G remains unchanged, α_G significantly surpasses the control mirroring elevated amount of SL-rich gel domains (Fig. 5, inset). The higher amount of highly ordered microdomains is in full agreement with findings of Riezman group, who reported 38% increase of SL levels in membranes of cells fed with exogenous DHS [20]. Reversibility and a rate of the observed changes indicate that the cell wall does play significant role in the reported effects and does not bias t-PnA emission.

4. Discussion

In this study, we combined measurements with two widely used reporters of membrane order, DPH and t-PnA, to characterize changes in the plasma membrane organization induced by variations in SL levels. Each dye incorporates into the membrane in a specific manner: while t-PnA is anchored at the membrane surface and its tetraene fluorophore penetrates not deeper than to the 8th–15th carbon of surrounding acyl-chains, which in SL typically contain 26 carbons, DPH floats freely in the membrane core and reaches even its less ordered central part. Existence of a transmembrane lipid-order gradient was documented earlier by both fluorescence and magnetic resonance [31,32]. Accordingly, DPH reported lower limiting anisotropies as compared to t-PnA (compare Supplementary Table S1 and Table 2).

Both DPH and t-PnA registered massive SL depletion in *lcb*1-100 cells. This was manifested as a significant decrease in overall membrane order reported by DPH fluorescence anisotropy (Fig. 2). Surprisingly, t-PnA anisotropy decays in wild type and *lcb*1-100 cells revealed similar r_∞ for both gel and liquid membrane fractions (Table 2). This indicates that order of both solid and liquid parts of the membrane remained unaffected, just their relative proportions changed. The latter conclusion is supported also by t-PnA intensity decays, where low SL levels in *lcb*1-100 and myriocin-treated cells resulted in reduction of long-lifetime amplitude (Figs. 3 and 5). The decrease in SL in *lcb*1-100 cells is

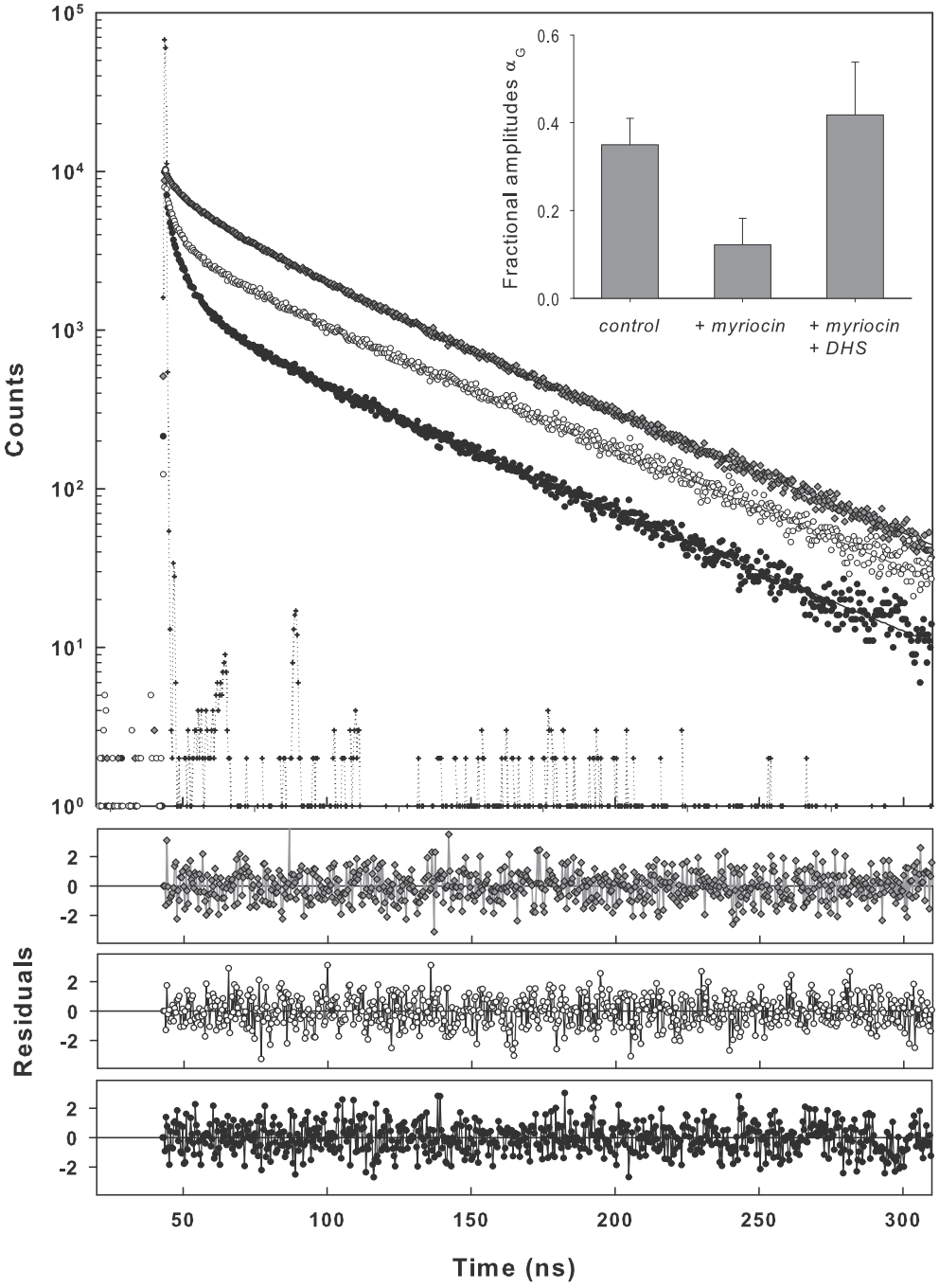

Fig. 5. Effect of SL levels on fluorescence decays of t-PnA. Levels of SL in wild type cells (○) were decreased by myriocin (5 μM, 2 h incubation, ●) and restored back by exogenous DHS (20 μM, 2 h incubation, gray diamonds). Solid lines represent the best fit and crosses impulse response function. Inset: fractional amplitudes of the gel-phase component.

Table 3
Fluorescence decay parameters of t-PnA in plasma membranes treated with myriocin and DHS.

	τ_{mean} (ns)[a]	α_1	τ_1 (ns)	α_2	τ_2 (ns)	α_3	τ_3 (ns)	α_4	τ_4 (ns)	α_G	τ_G (ns)	f_G[b]
Control	49.1	0.25	2.3	0.26	4.6	0.14	18.1	–	–	**0.35**[c]	**57.1**	0.82
Myriocin	40.5	0.44	1.7	0.31	5.7	0.09	14.1	0.04	38.0	**0.12**[c]	**58.3**	0.58
DHS	48.2	0.13	3.2	0.17	9.9	–	–	0.28	31.0	**0.42**[d]	**57.9**	0.69

[a] τ_{mean} was calculated using Eq. (S3); S.D. < 0.05 ns.
[b] The intensity fraction was calculated using Supplementary Eq. (S4).
[c] S.D. < 0.06.
[d] S.D. < 0.12.

reflected exclusively in reduction of the abundance of gel-like domains, while the order of liquid domains does not change. Biological impact of this finding is straightforward: the cells are able to preserve a minimal membrane order – the parameter which determines membrane permeability and, consequently, cell viability – even after almost 3-fold [20] drop in SL levels.

We show that the abundance of gel-like domains was restored in cells with blocked sphingolipid biosynthesis, when supplied with exogenous DHS (Fig. 5). Recently, Aresta-Branco et al. [14] observed significant reduction of these domains in cells lacking sphingolipid alpha-hydroxylase Scs7. Plasma membranes of *scs7Δ* cells exhibit normal lipid composition with a specific exception: drastically reduced levels of hydroxylated ceramides and complex SL are mirrored in almost identical increases in ceramides lacking a hydroxyl group on the fatty-acyl chain [13]. Altogether, these data strongly support the idea that SL themselves constitute highly ordered microdomains in the plasma membrane of living cells.

The method we used does not allow for localization of the S_o microdomains in the frame of the so far identified microdomain architecture of the yeast plasma membrane. We can only speculate that they will be excluded from ergosterol-enriched membrane compartment of Can1 (MCC). On the other hand, sphingolipids are required for plasma membrane trafficking and function of proton ATPase Pma1 and could stay associated with this most abundant protein of the yeast plasma membrane. SL-enriched S_o domains would be, therefore, a hot candidate for structural correlate of membrane compartment of Pma1 (MCP; [7] and citations therein). It has to be emphasized that the degree of order in these microdomains highly exceeds that of the hypothesized lipid rafts enriched in sterols and SL. Following the raft analogy, SL-based gel-like domains represent rather solid ice-floes in the otherwise fluid membrane.

Acknowledgments

The authors are grateful to Widmar Tanner for his inspired ideas and permanent encouragement, and Miroslava Opekarova for critical reading of the manuscript. t-PnA was a kind gift of Prof. F. Zsila from the Institute of Biomolecular Chemistry, Chemical Research Center, Budapest, Hungary. This work was supported by the Czech Science Foundation, project GACR P205/12/0720.

Appendix A. Supplementary data

Supplementary data associated with this article can be found, in the online version, at http://dx.doi.org/10.1016/j.febslet.2013.11.038.

References

[1] Dickson, R.C., Sumanasekera, C. and Lester, R.L. (2006) Functions and metabolism of sphingolipids in *Saccharomyces cerevisiae*. Prog. Lipid Res. 45, 447–465.
[2] Stancevic, B. and Kolesnick, R. (2010) Ceramide-rich platforms in transmembrane signaling. FEBS Lett. 584, 1728–1740.
[3] Ipsen, J.H., Karlstrom, G., Mouritsen, O.G., Wennerstrom, H. and Zuckermann, M.J. (1987) Phase equilibria in the phosphatidylcholine-cholesterol system. Biochim. Biophys. Acta 905, 162–172.
[4] Lingwood, D. and Simons, K. (2010) Lipid rafts as a membrane-organizing principle. Science 327, 46–50.
[5] Simons, K. and Gerl, M.J. (2010) Revitalizing membrane rafts: new tools and insights. Nat. Rev. Mol. Cell Biol. 11, 688–699.
[6] Ziolkowska, N.E., Christiano, R. and Walther, T.C. (2012) Organized living: formation mechanisms and functions of plasma membrane domains in yeast. Trends Cell Biol. 22, 151–158.
[7] Malinsky, J., Opekarova, M., Grossmann, G. and Tanner, W. (2013) Membrane microdomains, rafts, and detergent-resistant membranes in plants and fungi. Annu. Rev. Plant Biol. 64, 501–529.
[8] Kraft, M.L. (2013) Plasma membrane organization and function: moving past lipid rafts. Mol. Biol. Cell 24, 2765–2768.
[9] Spira, F., Mueller, N.S., Beck, G., von Olshausen, P., Beig, J. and Wedlich-Soldner, R. (2012) Patchwork organization of the yeast plasma membrane into numerous coexisting domains. Nat. Cell Biol. 14, 640–648.
[10] Thompson, J.E., Fernando, M.A. and Pasternak, J. (1979) Induction of gel-phase lipid in plasma membrane of chick intestinal cells after coccidial infection. Biochim. Biophys. Acta 555, 472–484.
[11] Welti, R., Rintoul, D.A., Goodsaid-Zalduondo, F., Felder, S. and Silbert, D.F. (1981) Gel phase phospholipid in the plasma membrane of sterol-depleted mouse LM cells. Analysis by fluorescence polarization and x-ray diffraction. J. Biol. Chem. 256, 7528–7535.
[12] Wolf, D.E., Maynard, V.M., McKinnon, C.A. and Melchior, D.L. (1990) Lipid domains in the ram sperm plasma membrane demonstrated by differential scanning calorimetry. Proc. Natl. Acad. Sci. USA 87, 6893–6896.
[13] Guan, X.L. and Wenk, M.R. (2006) Mass spectrometry-based profiling of phospholipids and sphingolipids in extracts from *Saccharomyces cerevisiae*. Yeast 23, 465–477.
[14] Aresta-Branco, F., Cordeiro, A.M., Marinho, H.S., Cyrne, L., Antunes, F. and de Almeida, R.F. (2011) Gel domains in the plasma membrane of *Saccharomyces cerevisiae*: highly ordered, ergosterol-free, and sphingolipid-enriched lipid rafts. J. Biol. Chem. 286, 5043–5054.
[15] Ruggiero, A. and Hudson, B. (1989) Analysis of the anisotropy decay of trans-parinaric acid in lipid bilayers. Biophys. J. 55, 1125–1135.
[16] Silva, L., De Almeida, R.F.M., Fedorov, A., Matos, A.P.A. and Prieto, M. (2006) Ceramide-platform formation and -induced biophysical changes in a fluid phospholipid membrane. Mol. Membr. Biol. 23, 137-U2.
[17] Silva, L.C., de Almeida, R.F.M., Castro, B.M., Fedorov, A. and Prieto, M. (2007) Ceramide-domain formation and collapse in lipid rafts: membrane reorganization by an apoptotic lipid. Biophys. J. 92, 502–516.
[18] Lentz, B.R. (1993) Use of fluorescent probes to monitor molecular order and motions within liposome bilayers. Chem. Phys. Lipids 64, 99–116.
[19] Munn, A.L. and Riezman, H. (1994) Endocytosis is required for the growth of vacuolar H(+)-ATPase-defective yeast: identification of six new END genes. J. Cell Biol. 127, 373–386.
[20] Zanolari, B., Friant, S., Funato, K., Sutterlin, C., Stevenson, B.J. and Riezman, H. (2000) Sphingoid base synthesis requirement for endocytosis in *Saccharomyces cerevisiae*. EMBO J. 19, 2824–2833.
[21] Jahnig, F. (1979) Structural order of lipids and proteins in membranes: evaluation of fluorescence anisotropy data. Proc. Natl. Acad. Sci. USA 76, 6361–6365.
[22] Castro, B.M., de Almeida, R.F., Silva, L.C., Fedorov, A. and Prieto, M. (2007) Formation of ceramide/sphingomyelin gel domains in the presence of an unsaturated phospholipid: a quantitative multiprobe approach. Biophys. J. 93, 1639–1650.
[23] Castro, B.M., Silva, L.C., Fedorov, A., de Almeida, R.F. and Prieto, M. (2009) Cholesterol-rich fluid membranes solubilize ceramide domains: implications for the structure and dynamics of mammalian intracellular and plasma membranes. J. Biol. Chem. 284, 22978–22987.
[24] Sklar, L.A., Hudson, B.S. and Simoni, R.D. (1977) Conjugated polyene fatty acids as fluorescent probes: synthetic phospholipid membrane studies. Biochemistry 16, 819–828.
[25] Mateo, C.R., Brochon, J.C., Pilar Lillo, M. and Ulises Acuna, A. (1993) Lipid clustering in bilayers detected by the fluorescence kinetics and anisotropy of trans-parinaric acid. Biophys. J. 65, 2237–2247.
[26] Mateo, C.R., Lillo, M.P., Gonzalezrodriguez, J. and Acuna, A.U. (1991) Lateral heterogeneity in human platelet plasma-membrane and lipids from the time-resolved fluorescence of trans-parinaric acid. Eur. Biophys. J. 20, 53–59.
[27] Vecer, J. and Herman, P. (2011) Maximum entropy analysis of analytically simulated complex fluorescence decays. J. Fluoresc. 21, 873–881.
[28] Mateo, C.R., Acuna, A.U. and Brochon, J.C. (1995) Liquid-crystalline phases of cholesterol lipid bilayers as revealed by the fluorescence of trans-parinaric acid. Biophys. J . 68, 978–987.
[29] Miyake, Y., Kozutsumi, Y., Nakamura, S., Fujita, T. and Kawasaki, T. (1995) Serine palmitoyltransferase is the primary target of a sphingosine-like immunosuppressant, Isp-1/myriocin. Biochem. Biophys. Res. Commun. 211, 396–403.
[30] Horvath, A., Sutterlin, C., Manning-Krieg, U., Movva, N.R. and Riezman, H. (1994) Ceramide synthesis enhances transport of GPI-anchored proteins to the Golgi apparatus in yeast. EMBO J. 13, 3687–3695.
[31] Seelig, J. and Waespesarcevic, N. (1978) Molecular order in cis and trans unsaturated phospholipid bilayers. Biochemistry 17, 3310–3315.
[32] Herman, P., Konopasek, I., Plasek, J. and Svobodova, J. (1994) Time-resolved polarized fluorescence studies of the temperature adaptation in Bacillus subtilis using DPH and TMA-DPH fluorescent probes. Biochim. Biophys. Acta 1190, 1–8.